Ultrasound in Med. & Biol., Vol. 41, No. 7, pp. 1927–1937, 2015

Printed in the USA
0301-5629

http://dx.doi.org/10.1016/j.ultrasmedbio.2015.03.020

● *Original Contribution*

BIOLOGICALLY AND ACOUSTICALLY COMPATIBLE CHAMBER FOR STUDYING ULTRASOUND-MEDIATED DELIVERY OF THERAPEUTIC COMPOUNDS

Dario Carugo, Joshua Owen, Calum Crake, Jeong Yu Lee, and Eleanor Stride
Department of Engineering Science, Institute of Biomedical Engineering, University of Oxford, Oxford, United Kingdom

(*Received* 19 *December* 2014; *revised* 13 *February* 2015; *in final form* 18 *March* 2015)

Abstract—Ultrasound (US), in combination with microbubbles, has been found to be a potential alternative to viral therapies for transfecting biological cells. The translation of this technique to the clinical environment, however, requires robust and systematic optimization of the acoustic parameters needed to achieve a desired therapeutic effect. Currently, a variety of different devices have been developed to transfect cells *in vitro*, resulting in a lack of standardized experimental conditions and difficulty in comparing results from different laboratories. To overcome this limitation, we propose an easy-to-fabricate and cost-effective device for application in US-mediated delivery of therapeutic compounds. It comprises a commercially available cell culture dish coupled with a silicon-based "lid" developed in-house that enables the device to be immersed in a water bath for US exposure. Described here are the design of the device, characterization of the sound field and fluid dynamics inside the chamber and an example protocol for a therapeutic delivery experiment. (E-mail: eleanor.stride@eng.ox.ac.uk) **© 2015 The Authors. Published by Elsevier Inc. on behalf of World Federation for Ultrasound in Medicine & Biology. This is an open access article under the CC BY-NC-ND license (http://creativecommons.org/licenses/by-nc-nd/4.0/).**

Key Words: **Ultrasound-mediated drug delivery, Small interfering RNA, *In vitro* assay, Cell culture device, Sonoporation.**

INTRODUCTION

The transfection of cells has enormous potential for the treatment of cancer and other major diseases. Currently, however, the low permeability of cell membranes to genetic materials represents a major hindrance to its clinical application. Viral vectors have been found to significantly improve intracellular delivery, but their use is limited by the risk of immunogenic responses and/or off-target effects (Edelstein et al. 2007). Non-viral transfection methods have consequently been investigated extensively; but, to date, the majority has yielded relatively low transfection efficiencies and/or unacceptable loss of cell viability (Glover et al. 2005). One method that has shown promise is the use of focused ultrasound (US) in combination with microbubble contrast agents. Under US exposure, the oscillation of the microbubbles induces a temporary permeabilization of nearby cell membranes via a process known as sonoporation (Lentacker et al. 2014). This technique has been used to deliver a variety of therapeutic compounds including small molecule drugs (Escoffre et al. 2011), deoxyribonucleic acid (DNA) (Miller et al. 2002) and small interfering RNA (siRNA) (Kinoshita and Hynynen 2005). However, much better understanding of the governing biophysical mechanisms and optimization of the exposure conditions for particular applications are required for development into a clinically relevant procedure. These, in turn, require the development of robust and reproducible experimental methods for generating and analyzing US-mediated cell transfection *in vitro*. Notably, no device has been designed specifically to fulfill this aim, and in most cases, devices developed for another purpose have been adapted to transfect cells via sonoporation, leading to significant variability between different studies.

On the basis of their geometry/architecture, devices can be classified in three main categories: (i) tubes, (ii) well plates or chambers and (iii) parallel-plate chambers (the most commonly used being OptiCell from Thermo Fisher Scientific, Waltham, MA, USA). Coupling of plastic round-bottom tubes (Fechheimer et al. 1987) and

Address correspondence to: Eleanor Stride, Department of Engineering Science, Institute of Biomedical Engineering, University of Oxford, Old Road Campus Research Building, Oxford OX3 7 DQ, UK. E-mail: eleanor.stride@eng.ox.ac.uk

commercially available tissue culture tubes (Ogawa et al. 2002) with US transducers has been reported for transfection of mammalian cells. Although simple to use, these devices are largely limited to the treatment of cells in suspension, and it is difficult to predict the acoustic field in the target region, particularly if acoustic standing waves are generated as a result of reflection from the tube walls, a problem particularly in low-aspect-ratio tubes. Similar problems may occur in well plates and cylindrical chambers coupled with piezo-electric transducers that have been used to investigate accumulation of drugs such as paclitaxel and doxorubicin in endothelial and cancer cells (Jackson et al. 2011) and to evaluate the biological response of cells undergoing sonoporation (Schlicher et al. 2006; Zhong et al. 2011). Well plates are particularly suitable for multiparametric studies as they provide the advantage of fast, post-sonication readouts, for example, using automatic plate readers. However, they suffer from limited flexibility with respect to the alignment of the US source and the significant mismatch in acoustic impedance between cell medium and the constitutive materials (*i.e.*, polystyrene [Bruus 2012]) and/or the air–water interface when insonified from below. The latter remains a problem even when plates with a flexible surface membrane (*e.g.*, BioFlex by Flexcell International, Burlington, NC, USA) are used.

In recent years, parallel-plate chambers have attracted increasing interest in the biomedical US community as a means of investigating US-mediated intracellular drug delivery in a physiologically relevant, confined environment. In particular, the OptiCell cell culture device (now discontinued) was previously used to systematically investigate transfection efficiency under varying acoustic conditions (Rahim et al. 2006), to optimize US-mediated targeted gene delivery via microbubbles to cultured primary endothelial cells (Meijering et al. 2007) and to examine the impact of molecular weight on the mechanism of molecular entry into primary endothelial cells (Meijering et al. 2009). Furthermore, acoustic and magnetic fields in combination have been used for intracellular gene delivery with this system (Stride et al. 2009). Despite their widespread usage, parallel-plate chambers may suffer from a range of drawbacks, including the recurrence of obstructions; the potential for generating high wall shear stresses during priming, which could compromise cell viability; difficulty in removing exogenous, trapped air bubbles; and the need for extracting cells post-sonication for culturing or analysis purposes.

Other methods have also been devised for examining US-mediated therapeutic delivery. For example Hu et al. (2013) developed a cell chamber integrated with a waveguide to sonoporate cells while observing membrane perforation and recovery using confocal microscopy. Karshafian et al. (2010) used an exposure chamber with two Mylar windows to investigate if sonoporation is limited by the size of the macromolecule to be delivered. Agar phantoms with a cavity have also been developed to examine the correlation between acoustic cavitation and cell viability (Lai et al. 2006). However, as these systems are application specific and not commercially available, they could be difficult to easily reproduce on a large scale.

With the aim of overcoming the limitations of previous systems, we have developed an easy-to-use, biologically and acoustically compatible device for application in US-mediated delivery of therapeutic compounds. It comprises a commercially available cell culture dish coupled with an acoustically compatible "lid" developed in-house that enables the dish to be immersed in a water bath for US exposure. The ease of fabrication and operation, together with its compatibility with standard cell culturing techniques and analytical instruments, makes it suitable for widespread application in different laboratory settings, potentially opening the way for the adoption of standard experimental protocols in the field of *in vitro* US-mediated delivery of therapeutic compounds. To facilitate the replication of the device by different laboratories, in addition to the description below, the full technical drawings and fabrication instructions are freely available on-line (www.sonofluidics.co.uk).

METHODS

Lid design and fabrication

The lid was fabricated in polydimethylsiloxane (PDMS) via replica moulding. PDMS has been extensively used for fabricating microfluidic devices, mainly because of its biocompatibility (Leclerc et al. 2003; Sia and Whitesides 2003), optical transparency (Whitesides 2006), permeability to gases (Zanzotto et al. 2004) and ease of moulding (Prebiotic 1995).

For this purpose, a manifold was constructed comprising three main components (Fig. 1a): (i) circular base plate (84 mm in diameter, 10 mm thick); (ii) 6.3-mm-thick disk with a step-like variation in diameter (*i.e.*, from 34 to 33 mm); and (iii) 49-mm-inner-diameter ring. Individual components were designed using SolidWorks 2012 (Dassault Systèmes SolidWorks, France) and fabricated in either Teflon or poly(methyl methacrylate) (PMMA) using a lathe machine (Weiler Praktikant VCD, Weiler, Emskirchen/Mausdorf, Germany). The three components were assembled in a single manifold by inserting the ring and the disk into two recesses milled within the base plate. Two segments of 1.6-mm–outer diameter polyether ether ketone (PEEK) rod (IDEX, Lake Forest, IL, USA) were glued to the top surface of the disk. Two circular recesses (0.5 mm deep) were milled on the disk surface to facilitate positioning of the rods.

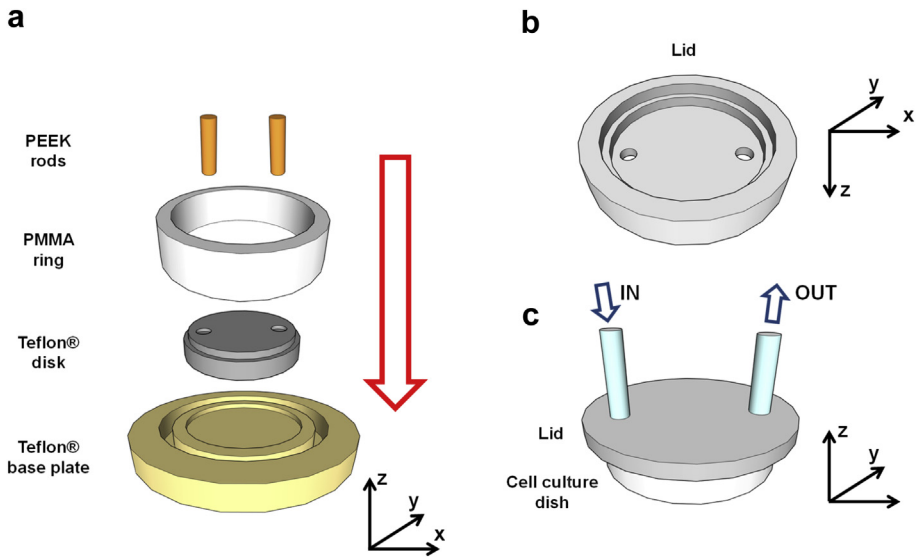

Fig. 1. Lid design and fabrication. (a) Components of the manifold constructed for replica moulding of the lid. These include a Teflon base plate with recesses for coupling with a Teflon disk and a PMMA ring, and two PEEK rods to be coupled with the top surface of the disk. The *red arrow* indicates the direction of assembly. (b) Schematic depiction of the obtained lid (shown inverted), with holes for fluid injection and discharge. (c) Lid coupled with a cell culture dish (*white*), with inlet and outlet Tygon tubing (*light blue*) inserted through its holes. PMMA = poly(methyl methacrylate); PEEK = polyether ether ketone.

Degassed, liquid PDMS (curing agent:monomer ratio = 1:10 w/w; Sylgard 184, Dow Corning, Corning, NY, USA) was poured into the assembled manifold. A scale bar was placed on the ring to vary the volume of PDMS so as to obtain the desired thickness of the lid. The manifold was subsequently placed on a hot plate (at 90°C, for 90 min) to allow the PDMS to set. Once solidified, the PDMS component was removed by deassembling the manifold into its individual parts. Notably, the disk acted as a positive mold to define the inner features of the lid (Fig. 1b), whereas the two segments of PEEK rod generated channels through the PDMS for delivery/discharge of fluids and cells. The resulting lid was then coupled with a cell culture dish (μ-Dish 35 mm, Ibidi, Munich, Germany), and connected to 1-cm-long inlet/outlet Tygon tubing (2.4-mm outer diameter, 1.2-mm inner diameter, Cole–Parmer Instrument, London, UK) for injection and discharge of fluid (Fig. 1c). Lids with different thicknesses (1.22, 2.23, 3.33, 4.30 and 5.87 mm), measured using a Vernier caliper, were fabricated. For applications involving biological cells, the lid (including connection tubing) was sterilized by overnight immersion in a solution of ethanol in deionized water (70% by volume) (Mata et al. 2005).

Functional characterization

Functional tests were performed to determine (i) the flow field within the cell culture dish, (ii) the sealing and (iii) acoustic characteristics of the lid and (iv) the biocompatibility and utility of the device for US-mediated cell transfection.

Numerical simulation of the internal flow field. A 3-D numerical model was developed to characterize the flow field within the cell culture dish during priming, to verify that: (i) the wall shear stress at the bottom surface of the cell dish was not large enough to impart cell damage, and (ii) regions of potential entrapment for exogenous air bubbles (*i.e.*, vortices) were not present. ICEM CFD 14.0 (Ansys, Canonsburg, PA, USA) was employed for construction and meshing of the model geometry (Supplemental Fig. 1a) (for all supplementary material, see the on-line version at http://dx.doi.org/10.1016/j.ultrasmedbio.2015.03.020). The geometry was meshed using tetrahedral cells (total number of elements = 1,780,448). The maximum mesh element size was set at 0.05 mm at the inlet and outlet boundaries, and 0.5 mm at the wall boundaries, with a 10-layer transition between-layer transition between the two (Supplemental Fig. 1b). The mass conservation equation

$$\nabla \cdot (\mathrm{v}) = 0 \tag{1}$$

and momentum conservation equation

$$\rho \frac{\partial \mathrm{v}}{\partial t} + \rho \mathrm{v} \cdot \nabla \mathrm{v} = -\nabla P + \mu \nabla^2 \mathrm{v} \tag{2}$$

where v, ρ, μ and P represent fluid velocity, density, dynamic viscosity and pressure, respectively, were solved over the computational flow domain, using Ansys Fluent 14.0 (Ansys, Canonsburg, PA, USA).

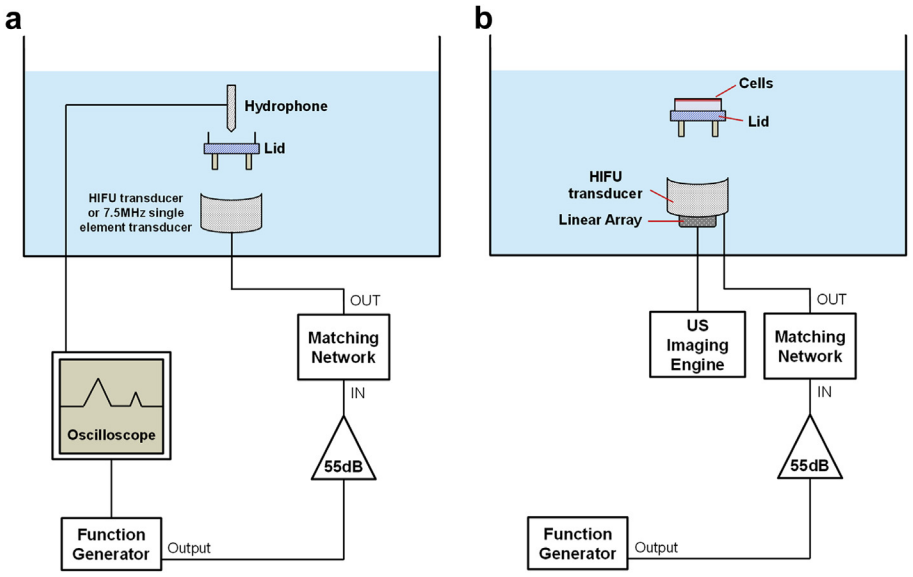

Fig. 2. Instrument setup for (a) measurement of lid acoustic characteristics and (b) US-mediated intracellular delivery of siRNA. HIFU = high intensity focused ultrasound; US = ultrasound; siRNA = small interfering RNA.

The working fluid was considered incompressible and Newtonian, with a density of 1000 kg/m^3 and a dynamic viscosity of 0.001 Pa·s. The flow was assumed to be steady and laminar. The semi-implicit method for pressure-linked equations (SIMPLE) algorithm was employed for solving the governing equations. Mass flow rate and zero-pressure boundary conditions were imposed at the inlet and outlet surfaces, respectively. A no-slip flow boundary condition was imposed on the other surfaces.

Lid sealing performance. The sealing performance of the lid was measured as follows: (i) a cell culture dish was weighed using a 0.1-mg (equivalent to ~0.1 μL of water)-resolution balance (Explorer Pro, Ohaus, Parsippany, NJ, USA); (ii) the dish was coupled to the lid and inlet/outlet ports were sealed; (iii) the device was submerged in a water tank for 15 min, at a depth of 10 cm from the free surface of the fluid, corresponding to an immersion depth for US transfection; (iv) the device was removed from the water tank and disassembled into its constituent components; and (v) the outer surface of the cell culture dish was dried using optical tissue wipers and the cell dish was weighed again. The percentage variation in mass was calculated as $(|m_{AS}-m_{BS}|)/m_{BS}$, where m_{BS} and m_{AS} are the average masses of the cell dish before (BS) and after (AS) submersion. Only values greater than 0.05% were considered to be significant with respect to experimental errors, and were associated with a leakage event. Lids with different thicknesses were tested with this method. A new cell dish was used for each individual experiment (n = 3), and each dish was weighed three times before and after submersion.

Lid acoustic characteristics. Tests were performed to quantify the attenuation and distortion of the sound field caused by the lid. Both the transmission of the incident field (typically ~0.5–1.5 MHz for therapeutic delivery) and the ability to detect acoustic emissions at higher frequencies (for cavitation detection and monitoring) were examined as described below.

Transmission of therapeutic excitation pulse (low frequency). Figure 2a is a schematic of the setup. The device was mounted on a custom-built holder and submerged in a water tank to enable efficient acoustic coupling and control of the internal liquid temperature (37°C for the experiments described here). Computer-controlled positioning stages, secured to an external frame, were employed to align the device with a piezo-electric transducer and a 0.4-mm-diameter needle hydrophone (HNA-0400, Onda, Sunnyvale, CA, USA). Transducers were supplied by Sonic Concepts (North Port, FL, USA); model H-107 F-18 was employed for US frequencies of 0.5 and 1.59 MHz, and model H-107 E-35 was employed for an US frequency of 1.1 MHz.

Transducers were actuated by a 55-dB power amplifier (A300, Electronics & Innovation, Rochester, NY, USA) driven by a sine wave from a programmable signal generator (33220A, Agilent Technologies, Santa Clara, CA, USA) and operated in pulsed mode (number of cycles = 100, period = 1 ms). The input voltage to the transducer was adjusted so as to obtain a maximum peak-to-peak acoustic pressure of 1 MPa at the focus (without a lid, *i.e.*, control test), for each US frequency investigated. A digital storage oscilloscope (44 Xi Waverunner, Teledyne LeCroy, Chestnut Ridge, NY, USA) was

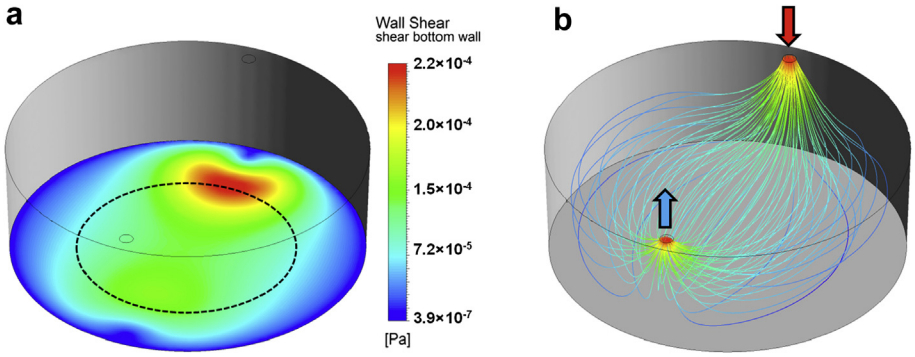

Fig. 3. Computational fluid dynamic characterization. (a) Contours of wall shear stress (in Pa) over the bottom surface of the cell dish (Q_{IN} = 1 mL/min). The *black dotted circle* corresponds to the region where cells are seeded. (b) Fluid streamlines within the cell dish (Q_{IN} = 1 mL/min). The *red and blue arrows* correspond to inlet and outlet boundaries, respectively.

used to monitor the input signal to the transducer and the output signal from the hydrophone.

To position the hydrophone precisely at the target plane (*i.e.*, where cells are located during transfection experiments), the bottom surface of the dish was removed. The hydrophone was operated in scanning mode, over a 4.8 × 4.8-mm area centered with respect to the target surface, and used to perform 32 measurements at each individual position. Maximum peak-to-peak acoustic pressure and the spatial characteristics of the sound field at the target plane were determined for different thicknesses of the lid and different US frequencies. Data were processed using MATLAB R2012a (The MathWorks, Natick, MA, USA).

Detection of high-frequency signal. To evaluate the performance of the lid at higher US frequencies (relevant, *e.g.*, for cavitation monitoring), the setup illustrated in Figure 2a was used again, but the transducer was replaced with a focused single-element transducer with a 7.5-MHz center frequency (V320-SU, Olympus NDT, Center Valley, PA, USA). The transducer was operated in burst mode (100 cycles per burst, pulse repetition frequency = 10 Hz) at frequencies of 4–11 MHz in steps of 1 MHz. A constant excitation voltage was used corresponding to 0.8-MPa peak-to-peak pressure at 8 MHz, falling to approximately 0.4 MPa at the extremes of the frequency range because of the frequency response of the transducer. Pressure values were subsequently normalized relative to free-field measurement without a lid. Thirty-two measurements were performed at the spatial peak at each frequency for five lids of different thicknesses. The same experimental setup, with minor adjustments, was used to measure the reflection coefficient for the lid and the substrate of the cell dish (see Supplemental Section 2).

Device performance for US-mediated cell transfection

The performance of the device in US-mediated cell transfection was tested using siRNA-loaded microbubbles. Details of the experimental procedure are reported below.

Production of siRNA loaded microbubbles. 1,2-Distearoyl-sn-glycero-3-phosphocholine (DSPC) and 1,2-distearoyl-*sn*-glycero-3-ethyl phosphocholine (DSEPC) from Avanti Polar Lipids (Alabaster, Alabama, USA) and polyethylene glycol (PEG)-40 stearate from Sigma–Aldrich (Gillingham, Dorset, UK) were dissolved in chloroform and mixed in a glass vial at molar ratio of 100:44:4.5. This mixture was heated to 50°C and left for 12 h to evaporate the chloroform. The resulting dry lipid film was suspended in filtered phosphate-buffered saline (10 mL) (Sigma–Aldrich) for 1 h at 75°C under constant stirring. The solution was then sonicated for 90 s to disperse the lipids using an ultrasonic cell disruptor (XL 2000, probe diameter 3 mm, 20 W, 22.5 kHz, Misonix, Farmingdale, NY, USA). Twenty microliters of Alexa Fluorophore 647-tagged siRNA oligo (absorption max: 650 nm, emission max: 668 nm) (Life Technologies, Paisley, UK) was added to the clear lipid suspension. The suspension was sonicated for 10 s with the probe immersed in the vial, followed by sonication at the air–water interface in the presence of sulfur hexafluoride to produce microbubbles. The suspension was then centrifuged (1000 rpm, 10 min) to remove any excess siRNA and examined via fluorescence microscopy with a Nikon Ti fluorescence microscope (Kingston upon Thames, Surrey, UK) using the far red filter combination (Cy5 HYQ), to determine whether siRNA had successfully attached to the microbubbles.

Preparation of cells for transfection experiments. An A549 human alveolar adenocarcinoma and an MCF-7 human breast adenocarcinoma cell line were used as representative biological models for transfection experiments in tumors. Cells were cultured in cell culture flasks using Dulbecco's Modified Eagle Medium (DMEM), supplemented with 10% fetal calf serum (FCS) from Sigma–Aldrich and 100 units/mL penicillin.

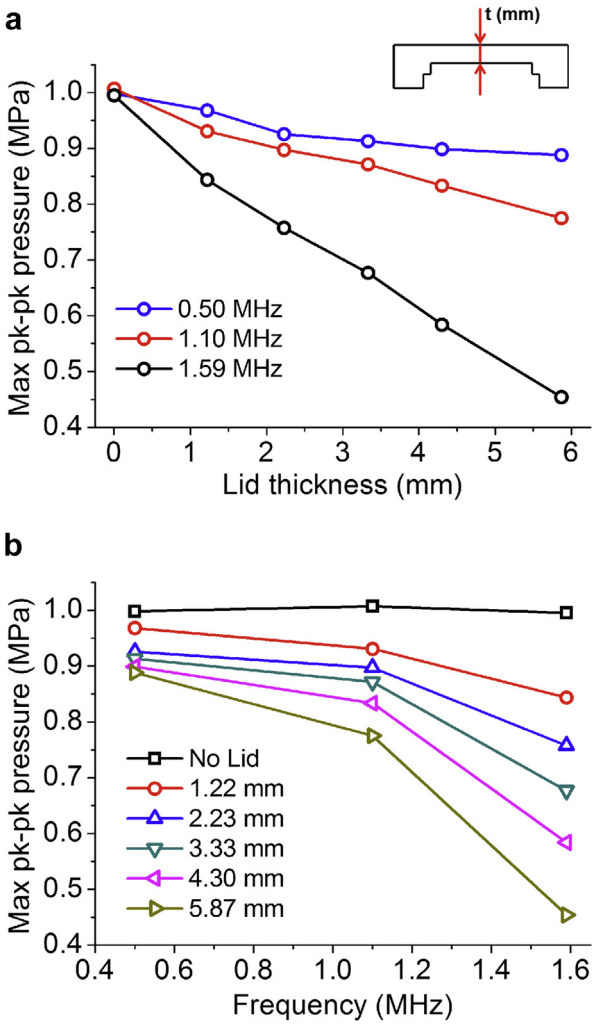

Fig. 4. (a) Maximum peak-to-peak pressure (in MPa) versus lid thickness (in mm), measured at three different ultrasound frequencies (*i.e.*, 0.5, 1.1 and 1.59 MHz) that are relevant for therapeutic applications. (b) Maximum peak-to-peak pressure (in MPa) versus frequency (in MHz), measured at different thickness values (in mm) of the lid. The inset in (a) is a cross-sectional view of the lid, with the location at which thickness (t) was measured (not to scale).

Cells were maintained at 37°C, 5% CO_2 in air with 95% humidity. When the cells were at confluence, they were trypsinized and resuspended in phenol-free medium within the cell dishes (μ-Dish 35 mm, Ibidi) at a concentration of 0.53×10^6 cells/mL. Cells were allowed to seed overnight in an incubator at 37°C before experimentation.

US-mediated transfection

Instrument setup. The instrumental setup is illustrated in Figure 2b. US was generated using a 0.5-MHz transducer with a 64-mm outer diameter, 63-mm focal length and 45 × 18-mm rectangular cutout for alignment of an imaging linear array probe (L10-5, Zonare Medical Systems, Mountain View, CA, USA). Driving waveforms were generated using a signal generator amplified by a 55-dB power amplifier and an impedance matching network as described above. The imaging probe had 128 elements, a 7.14-MHz center frequency and a 5-MHz bandwidth. The probe was used to verify that the US focus corresponded to the target plane, before exposing the cells.

US exposure experimental protocols. The culture dish was removed from the incubator and coupled with the lid. A 5-mL plastic syringe was connected to the inlet tubing to prime the dish with fresh medium. This was subsequently replaced with a 1-mL syringe for injection of the microbubble suspension. The outlet tubing was left open during these procedures to allow for removal of unwanted air pockets. Because the diameter of the inlet/outlet tubing (~1 mm) was larger than that of the needle (~0.7 mm) used for injecting the microbubbles, no significant effect on microbubble stability was expected. The inlet/outlet tubing was then sealed via insertion of a 5-mm-long segment of 1.6-mm-outside-diameter PEEK rod. The device was submerged in a water tank with the US transducer positioned below, allowing for the microbubbles to remain in close contact with the cells. The center of the cell-seeded surface was exposed to 40 cycles of 1-MPa (peak-to-peak) 0.5-MHz center frequency US at a 1-kHz pulse repetition frequency for a total of 10 s. Subsequently, the dish was removed from the water tank, the lid was de-coupled from the cell dish and cells were washed three times with phenol-free medium. Control tests were performed, to measure siRNA uptake in the absence of US. Cells were kept in phenol-free medium for examination by fluorescence microscopy.

Measurement of siRNA uptake via fluorescence microscopy. Fluorescence microscope images of cells were acquired using an inverted fluorescence microscope (Eclipse Ti-E, Nikon, Tokyo, Japan), equipped with an automated controller of the stage x–y position. The mean fluorescence intensity was determined for cells exposed to US in the presence of microbubbles, and compared with control tests (in the absence of US). Microscope images of cells were acquired, and the average fluorescence intensity was quantified using ImageJ (http://imagej.nih.gov/ij/index.html), over a 2.63 × 2.63-mm area concentric with the bottom surface of the dish at the focus of the US. Background subtraction was performed on each individual image.

RESULTS AND DISCUSSION

Functional characterization

Flow field characterization. Figure 3a illustrates the contours of fluid shear stress (in Pa) over the bottom surface of the dish, at a practical inlet volumetric flow rate

Table 1. Acoustic impedance of materials commonly used in the fabrication of devices employed in ultrasound-mediated intracellular drug delivery experiments, compared with the acoustic impedance of water and PDMS lid

Material	Device	Longitudinal speed of sound, c (m/s)	Density, ρ (kg/m^3)	Characteristic acoustic impedance, $Z = \rho c$ (N·s/m^3)
PDMS (Tsou et al. 2008)	Lid	1077	1028	1.107×10^6
Polystyrene (Bruus 2012)	OptiCell Well plates	2350	1050	2.468×10^6
Polypropylene (Lochab and Singh 2004)	Eppendorf tubes	2200	910	2.002×10^6
Agar (Culjat et al. 2010)		1498–1600	1016–1100	$1.52–1.76 \times 10^6$
Water (Leibacher et al. 2014)		1497	998	1.494×10^6

PDMS = polydimethylsiloxane.

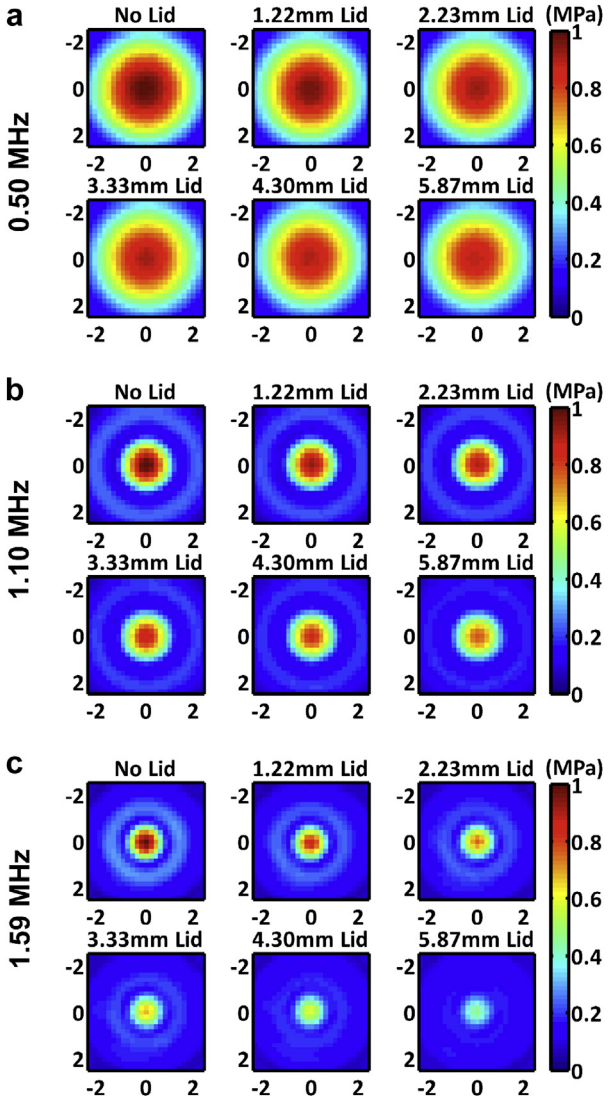

Fig. 5. (a–c) Contours of peak-to-peak acoustic pressure (in MPa) at the target plane (axes are in mm), measured at different thickness values of the lid, and US frequencies of 0.5 MHz (a), 1.1 MHz (b) and 1.59 MHz (c). The excitation voltage was adjusted to obtain a peak-to-peak focal pressure of 1 MPa for each ultrasound frequency.

(Q_{IN}) of 1 mL/min. The *black dotted line circle* indicates the area where cells are seeded. The shear stress in this region ranges from $\sim 6 \times 10^{-5}$ to $\sim 2 \times 10^{-4}$ Pa, which is significantly lower than values reported to induce cell detachment (Douville et al. 2011), reduce cell viability or elicit a biological response (Hua et al. 1993), which are of the order of 1 Pa. This is particularly important, as the effect of US and/or microbubbles should be decoupled from the effect of fluid shear stress during priming (Park et al. 2011). Notably, there appears to be a large margin for increasing the inlet flow rate—and, thus, reducing the priming time—without eliciting cell damage. Such flexibility in operation may not be achievable with parallel-plate chambers, which are usually considerably thinner (*i.e.*, 2 mm in the case of OptiCell), resulting in higher wall stress for a given priming flow rate.

Figure 3b illustrates the fluid streamlines within the device, at $Q_{IN} = 1$ mL/min. There is a notable absence of vortices within the cell dish during priming, except at very high flow rates, which is particularly important as vortices could act as entrapment sites for exogenous air bubbles. In contrast, vortices are likely to form within high-aspect-ratio flow cells, unless measures are taken to design appropriate connections with the inlet and outlet tubing (*i.e.*, tapered connections).

Sealing performance. Experiments were conducted to assess the sealing performance of the lid. This is particularly important, as the exchange of fluid between the cell dish and the surrounding environment could alter the osmotic properties of the cell medium, leading potentially to bacterial contamination and compromised cell viability. Lids of different thicknesses were tested. In all cases examined, the average percentage variation in cell dish mass was lower than 0.016% (which was lower than measurement uncertainty and, thus, indicated no leakage), with the exception of the 5.87-mm-thick lid for which the average percentage variation was 0.074%, likely because of the deflection of the lid's edges, resulting in less tight contact with the side walls of the cell dish.

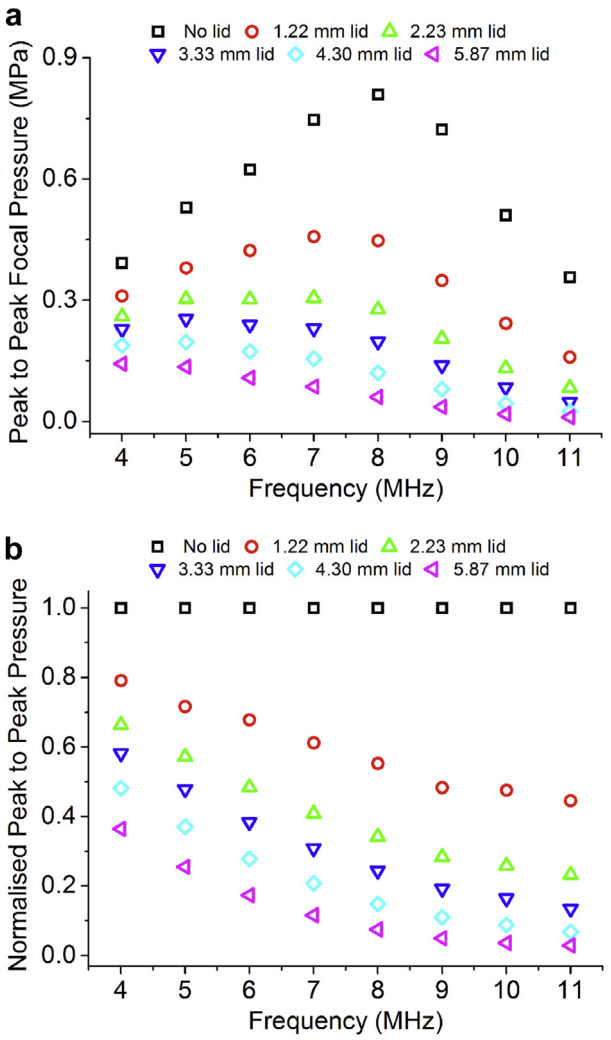

Fig. 6. (a) Absolute (in MPa) and (b) normalized peak-to-peak focal pressure for different lid thicknesses as a function of ultrasound frequency (in MHz).

Acoustic characteristics

Low-frequency US transmission. Experiments were performed to measure the potential attenuation and distortion of the sound field caused by the presence of the lid, at therapeutically relevant US frequencies in the range 0.50–1.59 MHz. A hydrophone was positioned at the target plane and operated in scanning mode over a 4.8 × 4.8-mm area centered with the bottom plane of the cell dish. Notably, the spatial characteristics of the sound field are of particular importance to verify the acoustic environment to which the cells will be exposed for therapeutic delivery. The maximum peak-to-peak acoustic pressure over this area was measured for different thicknesses of the lid and US excitation frequencies (Fig. 4). As expected, the maximum peak-to-peak acoustic pressure decreased with increasing thickness of the lid (Fig. 4a). At a frequency of 1.1 MHz. The maximum peak-to-peak acoustic pressure decreased from 0.931 MPa for a 1.22-mm-thick lid to 0.775 MPa for a 5.87-mm-thick lid. In most cases examined, the maximum peak-to-peak pressure was >90% of the maximum recorded value (*i.e.*, in the absence of the lid) (Fig. 4a).

Increasing the US excitation frequency resulted in increased attenuation of the incident field (Fig. 4b). For an average lid thickness of 3.33 mm, the maximum peak-to-peak acoustic pressure decreased from 0.913 MPa (at 0.50 MHz) to 0.872 MPa (at 1.10 MHz) and 0.677 MPa (at 1.59 MHz). The shape of the transmitted waveform was also examined, and it was found that the lid had a negligible effect over the range of transmit frequencies investigated (see Supplemental Section 3).

Results indicate that for the large majority of lid architectures and therapeutically relevant US frequencies investigated (*i.e.*, ∼1 MHz for sonoporation studies), the attenuation of the incident sound field was marginal and compatible with many applications. Importantly, given that the acoustic impedances of PDMS and water are very similar (see Table 1), there is negligible sound reflection at the water–PDMS interface (Leibacher et al. 2014). To confirm this, we measured the reflection coefficient for the thickest lid (see Supplemental Section 2), which was 0.033, whereas the reflection coefficient for the cell dish substrate was 0.078.

In contrast, the acoustic impedance of materials commonly used for fabricating well plates, cell culture dishes or parallel-plate chambers often differs significantly from the acoustic impedance of water (Table 1), posing some limitations to their use for US-mediated drug delivery experiments because of the difficulties in obtaining a well-defined and predictable acoustic environment and/or avoiding the formation of standing waves.

Figure 5 illustrates the contours of peak-to-peak acoustic pressure at the target plane for different lid thicknesses and US excitation frequencies. The spatial characteristics of the sound field are virtually undistorted under the range of experimental conditions investigated. As reported in Figure 4, attenuation of the sound field with increasing lid thickness and US frequency can be appreciated.

High-frequency transmission. The aim of this experiment was simply to test the possibility of detecting higher US frequencies and determine how attenuation relates to lid thickness, so as to evaluate the usability of the lid for applications in which detection of high-frequency components is needed. Therefore, single-point hydrophone measurements were made in the central region of the lid for each thickness. The results are illustrated in Figure 6. As expected, attenuation increased with US frequency and lid thickness.

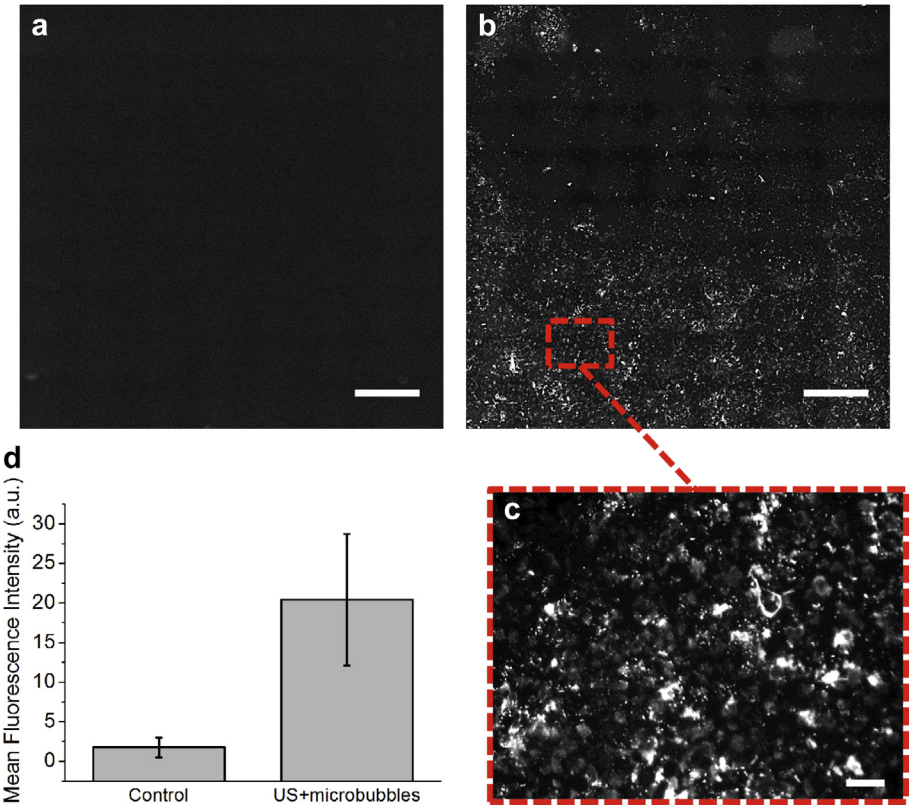

Fig. 7. US-mediated cell transfection. (a, b) Fluorescence microscope image of cells treated with small interfering RNA-functionalized microbubbles in the absence (a, control) and the presence (b) of US. Images correspond to a scan over a 2.63 × 2.63-mm area (10× objective). Bar = 400 μm. (c) Magnified view (20×) of cells treated with US. Bar = 40 μm. (d) Mean fluorescence intensity (a.u.) for both control test and sample exposed to US. Values are reported together with the standard error of the mean. n = 3; US = ultrasound.

Results from both the sealing and acoustic characterization tests suggest that an intermediate lid thickness (*i.e.*, in the range 2–3 mm) represents the optimal compromise between sealing and acoustic transmission at therapeutically relevant US frequencies. However, increased attenuation of the US field was observed at higher frequencies for all thicknesses, which could potentially limit the usability of the device—in its current configuration—for applications involving spatiotemporal detection of cavitation events (*i.e.*, via passive acoustic mapping [Jensen et al. 2012]). This is discussed further under Evaluation.

Device performance for US-mediated transfection

To illustrate the utility of the lid for in vitro experiments involving US-mediated delivery of therapeutic compounds, A459 human alveolar adenocarcinoma cells were grown within cell dishes and subsequently exposed to 0.5 MHz through the lid, in the presence and in the absence of siRNA-functionalized microbubbles.

Representative fluorescence microscope images of cells are provided in Figure 7a (control test) and Figure 7b and c (US + microbubbles). Figure 7d illustrates that siRNA was successfully delivered to the cells in the presence of microbubbles and US, as manifested in the increased mean fluorescence intensity (Fig. 7d). Cell viability was measured using fluorescence-activated cell sorting (FACS), and both transfected cells and control cells remained viable 24 h after US exposure, indicating the biocompatibility of the lid.

Evaluation

The device presented in this study comprises a biologically compatible cell dish coupled with an acoustically transparent lid, providing an easy-to-use chamber with well-defined exposure conditions for carrying out US mediated delivery experiments. It offers the following additional advantages: optical transparency (see Fig. 8 for representative cell imaging), gas permeability, possibility of large-scale fabrication via replica molding and compatibility with analytical instruments (*i.e.*, plate readers). The estimated cost of one device (lid and base) is approximately £3/US$4.50 at the time of writing (compared with, *e.g.*, £8/US$12.50 for a single OptiCell). Moreover, the lids can be easily sterilized and re-used multiple times without degradation of their mechanical

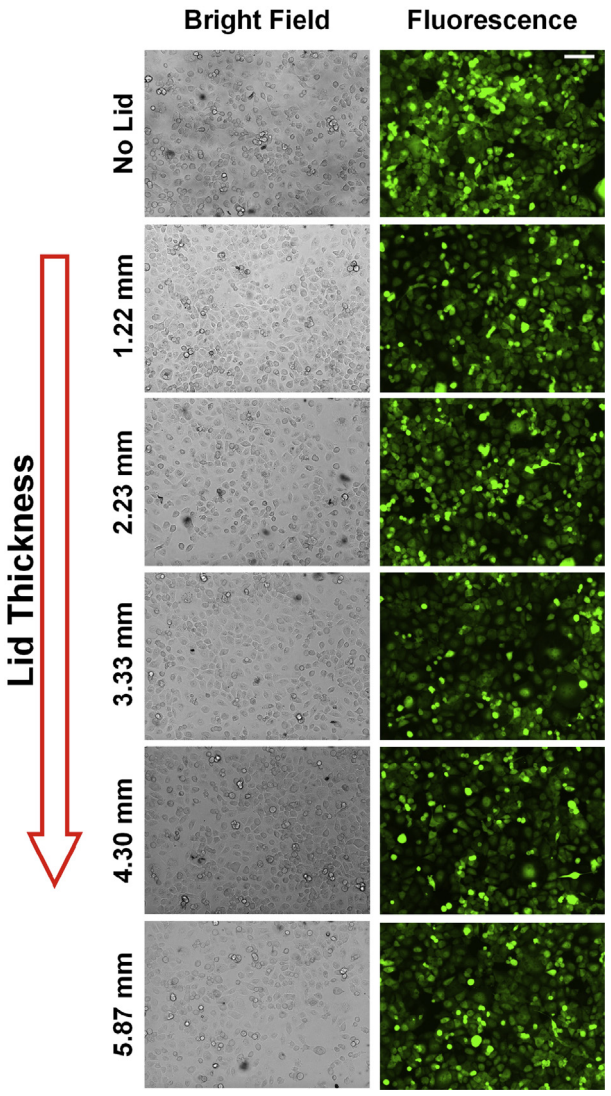

Fig. 8. Microscope imaging of cells within the device. Bright-field and fluorescence microscope images of GFP-expressing MCF7 cells within the device, acquired with the Nikon Ti fluorescence microscope (Kingston upon Thames, Surrey, UK). Camera exposure time was set to 0.8 and 300 ms for bright-field and fluorescence imaging, respectively. A 10× magnification objective was employed, and the digital gain was set to 0.8. Bar = 20 μm. GFP = green fluorescent protein.

or optical properties, as the PDMS formulation used in this study has been proven to be resistant to the sterilizing medium (i.e., ethanol) (Mata et al. 2005), which makes it an attractive option in many laboratory settings, opening the way for the adoption of common experimental protocols. To this end, technical drawings of the device and fabrication instructions will be made available on-line free of charge for interested users, together with future developments of the system (www.sonofluidics.co.uk).

One current drawback of the device is that the PDMS lid attenuates higher-frequency US which limits the use of cavitation detection protocols. However, future work is focused on designing a second-generation lid architecture that allows for both efficient US transmission into the cell dish and mapping of the spatial and temporal extent of cavitation whilst maintaining structural integrity. Future work will also focus on achieving a more predictable shear stress distribution on the dish surface so as to develop a platform for application of US under *in vivo* flow conditions. In addition, although acoustic reflections from the surface to which the cells were attached were found to be negligible in these experiments, the mechanical properties of the surface may affect the cavitation dynamics. This requires further investigation to increase the relevance of *in vitro* transfection experiments to *in vivo* work.

CONCLUSIONS

The US-mediated intracellular delivery of genetic material and therapeutic compounds has great potential in cancer therapy; however, it suffers from a lack of standardized protocols for investigating the governing mechanisms *in vitro* and optimizing exposure parameters. To address this issue, we have developed an easy-to-use device for application in US-mediated delivery of therapeutic compounds and have illustrated transfection of human alveolar adenocarcinoma cells using fluorescently tagged siRNA-loaded microbubbles.

Acknowledgments—We thank the Engineering and Physical Sciences Research Council for supporting the work through EP/I021795/1. Calum Crake acknowledges the support of RCUK Digital Economy Programme Grant EP/G036861/1 (Oxford Centre for Doctoral Training in Healthcare Innovation). We also thank James Fisk and David Salisbury for construction of the transducer and phantom holders used in this study.

SUPPLEMENTARY DATA

Supplementary data related to this article can be found at http://dx.doi.org/10.1016/j.ultrasmedbio.2015.03.020

REFERENCES

Bruus H. Acoustofluidics 2: Perturbation theory and ultrasound resonance modes. Lab Chip 2012;12:20–28.

Culjat MO, Goldenberg D, Tewari P, Singh RS. A review of tissue substitutes for ultrasound imaging. Ultrasound Med Biol 2010;36:861–873.

Douville NJ, Zamankhan P, Tung YC, Li R, Vaughan BL, Tai CF, White J, Christensen PJ, Grotberg JB, Takayama S. Combination of fluid and solid mechanical stresses contribute to cell death and detachment in a microfluidic alveolar model. Lab Chip 2011;11:609–619.

Edelstein ML, Abedi MR, Wixon J. Gene therapy clinical trials worldwide to 2007: An update. J Gene Med 2007;9:833–842.

Escoffre J, Piron J, Novell A, Bouakaz A. Doxorubicin delivery into tumor cells with ultrasound and microbubbles. Mol Pharm 2011;8:799–806.

Fechheimer M, Boylan JF, Parker S, Sisken JE, Patel GL, Zimmer SG. Transfection of mammalian cells with plasmid DNA by scrape loading and sonication loading. Proc Natl Acad Sci USA 1987;84:8463–8467.

Glover DJ, Lipps HJ, Jans DA. Towards safe, non-viral therapeutic gene expression in humans. Nat Rev Genet 2005;6:299–310.
Hu Y, Wan JMF, Yu ACH. Membrane perforation and recovery dynamics in microbubble-mediated sonoporation. Ultrasound Med Biol 2013;39:2393–2405.
Hua J, Erickson LE, Yiin TY, Glasgow LA. A review of the effects of shear and interfacial phenomena on cell viability. Crit Rev Biotechnol 1993;13:305–328.
Jackson JK, Pirmoradi FN, Wan CPL, Siu T, Chiao M, Burt HM. Increased accumulation of paclitaxel and doxorubicin in proliferating capillary cells and prostate cancer cells following ultrasound exposure. Ultrasonics 2011;51:932–939.
Jensen CR, Ritchie RW, Gyöngy M, Collin JR, Leslie T, Coussios CC. Spatiotemporal monitoring of high-intensity focused ultrasound therapy with passive acoustic mapping. Radiology 2012;262:252–261.
Karshafian R, Samac S, Bevan PD, Burns PN. Microbubble mediated sonoporation of cells in suspension: Clonogenic viability and influence of molecular size on uptake. Ultrasonics 2010;50:691–697.
Kinoshita M, Hynynen K. A novel method for the intracellular delivery of siRNA using microbubble-enhanced focused ultrasound. Biochem Biophys Res Commun 2005;335:393–399.
Lai CY, Wu CH, Chen CC, Li PC. Quantitative relations of acoustic inertial cavitation with sonoporation and cell viability. Ultrasound Med Biol 2006;32:1931–1941.
Leclerc E, Sakai Y, Fujii T. Cell culture in 3-dimensional microfluidic structure of PDMS (polydimethylsiloxane). Biomed Microdevices 2003;5:109–114.
Leibacher I, Schatzer S, Dual J. Impedance matched channel walls in acoustofluidic systems. Lab Chip 2014;14:463–470.
Lentacker I, De Cock I, Deckers R, De Smedt S, Moonen C. Understanding ultrasound induced sonoporation: Definitions and underlying mechanisms. Adv Drug Deliv Rev 2014;72:49–64.
Lochab J, Singh V. Acoustic behaviour of plastics for medical applications. Indian J Pure Appl Phys 2004;42:595–599.
Mata A, Fleischman AJ, Roy S. Characterization of polydimethylsiloxane (PDMS) properties for biomedical micro/nanosystems. Biomed Microdevices 2005;7:281–293.
Meijering BDM, Henning RH, Van Gilst WH, Gavrilovic I, Van Wamel A, Deelman LE. Optimization of ultrasound and microbubbles targeted gene delivery to cultured primary endothelial cells. J Drug Target 2007;15:664–671.
Meijering BDM, Juffermans LJM, Van Wamel A, Henning RH, Zuhorn IS, Emmer M, Versteilen AMG, Paulus WJ, Van Gilst WH, Kooiman K, De Jong N, Musters RJP, Deelman LE, Kamp O. Ultrasound and microbubble-targeted delivery of macromolecules is regulated by induction of endocytosis and pore formation. Circ Res 2009;104:679–687.
Miller DL, Pislaru SV, Greenleaf JF. Sonoporation: Mechanical DNA delivery by ultrasonic cavitation. Somatic Cell Mol Genet 2002;27:115–134.
Ogawa R, Kondo T, Honda H, Zhao QL, Fukuda S, Riesz P. Effects of dissolved gases and an echo contrast agent on ultrasound mediated in vitro gene transfection. Ultrason Sonochem 2002;9:197–203.
Park J, Fan Z, Deng CX. Effects of shear stress cultivation on cell membrane disruption and intracellular calcium concentration in sonoporation of endothelial cells. J Biomech 2011;44:164–169.
Prebiotic R. Polymer microstructures formed by moulding in capillaries. Nature 1995;376:581.
Rahim A, Taylor SL, Bush NL, ter Haar GR, Bamber JC, Porter CD. Physical parameters affecting ultrasound/microbubble-mediated gene delivery efficiency in vitro. Ultrasound Med Biol 2006;32:1269–1279.
Schlicher RK, Radhakrishna H, Tolentino TP, Apkarian RP, Zarnitsyn V, Prausnitz MR. Mechanism of intracellular delivery by acoustic cavitation. Ultrasound Med Biol 2006;32:915–924.
Sia SK, Whitesides GM. Microfluidic devices fabricated in poly(dimethylsiloxane) for biological studies. Electrophoresis 2003;24:3563–3576.
Stride E, Porter C, Prieto AG, Pankhurst Q. Enhancement of microbubble mediated gene delivery by simultaneous exposure to ultrasonic and magnetic Fields. Ultrasound Med Biol 2009;35:861–868.
Tsou JK, Liu J, Barakat AI, Insana MF. Role of ultrasonic shear rate estimation errors in assessing inflammatory response and vascular risk. Ultrasound Med Biol 2008;34:963–972.
Whitesides GM. The origins and the future of microfluidics. Nature 2006;442:368–373.
Zanzotto A, Szita N, Boccazzi P, Lessard P, Sinskey AJ, Jensen KF. Membrane-aerated microbioreactor for high-throughput bioprocessing. Biotechnol Bioeng 2004;87:243–254.
Zhong W, Sit WH, Wan JMF, Yu ACH. Sonoporation induces apoptosis and cell cycle arrest in human promyelocytic leukemia cells. Ultrasound Med Biol 2011;37:2149–2159.